Properties of quaternized and crosslinked carboxymethylcellulose films

Properties of quaternized and crosslinked carboxymethylcellulose films

Ivan Šimkovic • Filip Gucmann • Michal Hricovíni • Raniero Mendichi • Alberto Giacometti Schieroni • Daniele Piovani • Stefania Zappia • Edmund Dobročka • Jaroslav Filip • Miloš Hricovíni

I. Šimkovic (*) • M. Hricovíni • M. Hricovíni Institute of Chemistry, Slovak Academy of Sciences, 845 38 Bratislava, Slovakia e-mail: chemsimk@savba.sk

F. Gucmann • E. Dobročka Institute of Electrical Engineering, Slovak Academy of Sciences, Dúbravská cesta 9, 84104 Bratislava, Slovakia

R. Mendichi Expert Analysis, Molecular and Rheological Characterization Complex Polymers, Via Roma 7, 20067 Tribiano, Milan, Italy

A. G. Schieroni • D. Piovani • S. Zappia Instituto di Scienze e Tecnologie Chimiche “G. Natta”, Via A. Corti 12, 20133 Milan, Italy J. Filip Department of Environmental Protection Engineering, Faculty of Technology, Tomas Bata University, Zlín, Czechia

ABSTRACT

The sodium salt of carboxymethylcellulose (CMC Na) is a suitable water-soluble derivative for the preparation of quaternized and crosslinked films. In this study, we prepared quaternized and crosslinked films. In this study, we prepared quaternized and crosslinked CMC Na (QCCMC) films, along with only quaternized (QCMC) and only crosslinked CMC Na (CCMC) derivates, using one-step sythesis. The derivatives were characterized by high-resolution nuclear magnetic resonance (NMR) spectroscopy.

Size-exclusion chromatographic multi-angle laser light scattering (SEC-MALS) revealed the solubilities of the studied derivatives: CMC Na (98.Q%) > CCMC (81.2%) > QCMC (78.2%) > QCCMC (77.4%), while the gyration radii (R_g) of the polysaccharide coils were: CMC Na (20-78 nm) > QCCMC (2Q-65 nm) > QCMC (25-45 nm) > CCMC (24-4Q nm). Cyclic voltammetry distinguished all four types of derivatives with constant ΔE, I_a and I_c parameters. X-ray diffraction confirmed that all of the prepared films were in an amorphous state. PeakForce quantitative nanomechanical mapping (PF-QNM) was used to study the film surface morphology and film surface mechanical properties of all of the prepared carboxymethylcellulose derivatives. The following decreasing orders were found for root mean square surface films roughness: CCMC (6.5 nm) > CMC Na (6.4 nm) > QCMC (4.1 nm) > QCCMC (2.0 nm); films reduced elastic modulus: CCMC (9.3 GPa) > QCCMC (8.0 GPa) > CMC Na (7.0 GPa) > QCMC (2.1 GPa); films stiffness: CCMC (66.8 N/m) > CMC Na (55.4 N/m) > QCCMC (53.9 N/m) > QCMC (20.5 N/m) and films adhesion: CCMC (25.7 nN) > CMC Na (21.4 nN) > QCMC (17.1 nN) > QCCMC (11.5 nN).

Keywords: Sodium carboxymethyl cellulose (CMC Na) • Quaternized carboxymethyl cellulose (QCMC) • Crosslinked carboxymethyl cellulose (CCMC) • Quaternized and crosslinked carboxymethyl cellulose (QC-CMC) • Film properties

Introduction

Water-soluble cellulose derivatives like sodium salt of carboxymethylcellulose (CMC Na) represent optimal materials for the preparation of films (Zennifer et al. 2021; Wang et al. 2021). Their outstanding water-solubility, even after suitable action with crosslinking agents were introduced (Beghetto et al. 2020), represents the main advantage in a number of applications. Moreover, quaternization of CMC Na, i.e. introduction of quaternary ammonium group linked to polysaccharide species in the CMC Na form can be used to open new possibilities for the preparation of new combined water-soluble CMC Na derivatives. Further, our study described here confirmed, that when the CMC Na crosslinking with epichlorohydrin is used, a larger molecular weight can be achieved, while maintaining the similar water-solubility level. This way, a crosslinking bridge is formed with new free hydroxyl group. This approach represents an alternative for the preparation of hydrogels by mixing the CMC Na with quaternized cellulose (QC) and crosslinked cellulose (CC; Wei et al. 2021; Chai and Simonsen 2006; Chang et al. 2011). We consider this approach an improvement to previous cited reports, because the new formed hydroxypropyl bridge can enhance the mechanical properties due to formation of new hydrogen bonds in the macromolecule. Also important is the fact that the derivative remains water soluble, despite being crosslinked. In this work, we studied the quaternized/crosslinked CMC Na derivatives as the source film materials to find out how their properties can be affected. CMC Na is safe to be used as a food additive where due to its swelling properties can act as a viscosity modifier or thickening agent (Behra. et al. 2019). However, it is also widely used in cosmetic industry for manufacture of personal care products, for pharmaceutical applications or in water treatment (Javanbakht and Shaabani 2019). CMC Na can be produced from renewable sources such as e.g. softwood pulp or cotton linter which makes is a good alternative to some other materials. Crosslinking of the CMC Na can enhance its properties which may in turn enable its use in wider variety of applications, or it could increase their longevity. Expected crosslinking-improved mechanical properties of CMC Na-based films may contribute to better shelf-life of various commercial products, allow improved handling during the manufacture or may even help to cut down material costs in various packaging applications where thickness of films or extrusions could be decreased without compromising of their structural integrity. Currently, the knowledge of the surface morphology and mechanical properties of the crosslinked CMC Na films is limited. Standard mechanical testing may be difficult to carry out and produce less reliable data in case of film inhomogeneities. For this reason, we employed spatially-resolved nanomechanical mapping, which enabled us to compare all prepared films, similarly to our previous study on seaweed films (Simkovic et al. 2021).

All samples in this study were analyzed in solution by NMR and SEC-MALS analyses. Subsequently, films were prepared and tested by cyclic voltammetry, X-ray diffraction (XRD), atomic force microscopy (AFM)-derived PeakForce quantitative nanomechanical mapping (PF-QNM) with the goal to evaluate their properties and suitability for possible environ-mentally-friendly applications.

Experimental

Materials

Carboxymethylcellulose (CMC Na, 419,281, Sigma-Aldrich; M_w ~90,000 g/mol, degree of substitution (DS) ~ 0.7 CM group per anhydroglucose unit, m. p. = 274 °C (dec.); C, 34.57; H, 5.06); glycidyltri-methylammonium chloride (> 90%, 50053-50ML, GTMAC, Sigma-Aldrich); epichlorhydrin (99%, ALDRICH, E 105-5); sodium hydroxide (NaOH, SLAVUS), dialysis tubing (Union Carbide; 3.5 kDa MWCO), and other chemicals were used without further purifications.

Methods

All the NMR analyses were performed as described before (Šimkovic et al. 2020). In heteronuclear single quantum correlation total correlation spectroscopy (HSQC-TOCSY) experiments, data matrix was 1024 x 256 (F2 x F1), and zero-filled to 2 K x 1 K giving the final resolution of 2.9 Hz x 23.5 Hz. 90 ms-long DIPSI-2 sequence was used for Hartmann-Hahn mixing.

The elemental compositions were performed using a FLASH 2000 organic elemental analyzer (Thermo Fisher Scientific; furnace temperature: 950 °C; PTFE column, 6 mm o. d./5 mm i. d. X 2 m; 65 °C; helium was used as both carrier and reference gas with flows of 140 and 100 ml/min, respectively; oxygen flow was 250 ml/min; run time was 720 s; 12 s sampling delay; 5 s injection end).

The molecular weight distribution (MWD) and size of the macromolecules (radius of gyration, R_g) were obtained using an absolute multi-angle laser light scattering (MALS) detector connected to a size-exclusion chromatographic (SEC) system. We used 0.1 M Acetate buffer pH 4.5 solvent for the characterization of all samples and a modular multi-detector Alliance 2695 chromatographic system (Waters, USA). The Alliance SEC system was equipped with a MALS Dawn-DSP detector (Wyatt Technology, USA) and a 2414 differential refractometer (DRI) (Waters, USA) as a concentration detector. The experimental conditions were: three Shodex OHPak SB columns (806 HQ - 805 HQ - 804 HQ) (Showa Denko, Japan); 35 °C temperature; 0.8 ml/min flow rate;≈1.0 mg/ml sample concentration; refractive index increment dn/dc = 0.146 g/ml.

XRD patterns were acquired on a Bruker D8 DISCOVER diffractometer equipped with X-ray source with a rotating Cu anode operating at 12 kW. All measurements were performed in parallel beam geometry with a parabolic Goebel mirror in the primary beam (beam divergence ∼0.03°). Grazing incidence (GI) setup with constant angle of incidence α =2° and the angular range of 5° - 40° with step size of 0.05° and integration time of 1 s per step was used.

Surface morphology and PF-QNM analysis was performed using Bruker MultiMode 8-HR atomic force microscope, similar to previously described case (Simkovic et al. 2021). Silicon probes with the nominal spring constant K∼20-75 N/m were used (NCHV, supplied by Bruker, https://www.brukerafmp robes.com/p-3365-nchv.aspx). From each of the studied films, pieces of ∼1 X 1 cm were cut away and glued onto separate 12 mm diameter steel disc sample holders. Topography, spatially resolved mechanical properties (reduced elastic modulus and stiffness), and adhesion were evaluated from 3 to 5 locations across the sample surface to obtain representative films properties.

PF-QNM calibration and force curves analysis

Similar to our previous study (Simkovic et al. 2021), cantilever calibration was done do achieve quantitative nanomechanical results. First, cantilever deflection sensitivity was determined by approximation of the linear part of the force-displacement curve measured on the hard surface of the SAPPHIRE-12 M sample (Bruker); deflection sensitivity in the range of 44.0 ± 0.3 nm/V - 47.5 ± 0.3 nm/V was determined for the used cantilevers. The spring constant of the used cantilevers was determined by the Sader method (Sader et al. 2012, https://sadermethod.org), using measured cantilever resonance frequency and Q factor assuming free cantilever oscillations in air; values of 35.4 ± 3.6 N/m and 40.2 ± 4.1 N/m were obtained. The tip radius was obtained using tip qualification function of the Bruker Nanoscope Analysis software using a topography scan of the RS-12 M roughness test sample (Bruker), allowing the calculation of the effective tip radius as a function of indentation depth needed for the nanomechanical analysis. The same software was used to analyze the measured PF-QNM data;

cantilever deflection sensitivity, spring constant, and tip radius at the appropriate average indentation depth were used to determine the spatially resolved nanomechanical maps, i.e. reduced elastic modulus (E*), stiffness, and adhesion, applying the Johnson, Kendall, Roberts (JKR) theory (Johnson et al. 1971) to the force curves measured at every measured pixel. The reliability of the cantilever calibration was tested by a measurement on the PS-LDPE-12 M test sample (Bruker) with known mechanical properties with satisfactory results.

To avoid ambiguity, here we present values of reduced elastic modulus, instead of the true elastic modulus (E), since the values of Poisson's ratio (v) were unknown for the analyzed samples. The relation between true elastic and reduced modulus is described as: $E* = E_s/(1 - v_s^2)$, where v_s and E_s are the Poisson's ratio and the true elastic modulus of the sample, respectively. To avoid instrumentally-induced variations in the indentation depth, a constant force setpoint in the range ~20-50 nN (specific for each sample) was maintained during the PF-QNM data acquisition.

Electrochemical measurements

The samples were dissolved in deionized water (DW) to achieve 2 mg mL^{-1} solutions. These were dropped on working electrodes of screen printed electrodes (SPE; DropSens, Spain) in a volume of 30 µL. After drying in nitrogen stream, deposition of another 30 µL of polymer solution followed by drying in the nitrogen stream was performed. Such prepared electrodes were connected to PGSTAT 101 (Metrohm, Netherlands) potentiostat to perform cyclic voltammetry. Measurements were performed immediately after pipetting of 150 µL of 0.1 M phosphate buffer pH = 7.4 (PB) containing 10 mM ferricyanide on the modified SPE. All potentials are given against the Ag/ AgCl reference electrode of SPEs.

Crosslinking of CMC Na

CMC Na (10 mM) was mixed with water (90 mL; 5 M) containing NaOH (8 g; 0.2 M) and stirred at room temperature (RT) (1000 RPM, 2 h/RT), epichlo-rohydrin (ECH, 7.82 mL, 100 mM) was added and tempered (24 h/1000 RPM/60°C). The reaction was stopped by dilution with water, neutralized with HCl (from pH 12.6 to 8.85), then the solution was dialysed and lyophylized. The calculated yield of CCMC was 121% {[(dry weight of C-CMC/dry weight of CMC) x 100]; C, 37.39; H, 5.36} obtained.

Quaternization of CMC Na

CMC Na (10 mM) was mixed with water (90 mL; 5 M) containing NaOH (8 g; 0.2 M) and stirred (1000 RPM, 2 h/RT), before GTMAC (7.45 mL, 0.05 M) was added. After tempering at 60 °C/1000 RPM/24 h, the reaction was stopped by dilution with water (pH ~ 10.0), then the solution was dialyzed and lyophylized. The calculated yield of QCMC was 116% (dry weight of QCMC/dry weight of CMC) x 100; C, 38.84; H, 5.92; N, 1.45.

Quaternization/crosslinking of CMC Na

CMC Na (10mM) was mixed with water (90 mL; 5 M), containing NaOH (200 mM) and stirred (1000 RPM, 2 h/RT) and subsequently, GTMAC (7.45 mL, 50 mM) and ECH (7.82 mL, 100 mM) was added, and tempered at 60 °C/24 h at 1000 RPM. The reaction was stopped by dilution with water, attenuating

the pH to 10.3, then the solution was dialyzed and lyophylized. The calculated yield of QCCMC was 140% (dry weight of QC-CMC/dry weight of CMC Na) x 100; C, 43.38; H, 6.94; N, 2.21.

Films preparation

The films were prepared by mixing the CMC Na, and QCMC, CCMC, and QCCMC derivatives (0.25-0.5 g) with deionized water (∼50 ml), stirring (1000 RPM, 4 h/RT) and subsequent drying at RT (in plastic petri dishes) until a constant weight was reached.

Results and discussion

Chemical modification

The achieved yields of prepared derivatives were found to increase in the following order: QCMC (116%) < CCMC (121%) < QCCMC (140%); they were affected by the formation of new hydroxyl group on both the crosslinker and alkylating agent, both involved in second step crosslinking. The density of crosslinking was probably also affected by ionic interaction of carboxyls on CMC Na with the formed quaternary ammonium groups. This ionic interaction was also responsible for maintaing solubility of the formed CMC Na derivatives. The nitrogen content of QCCMC derivative (2.21%) was higher than of QCMC (1.45%). This confirms the hypothesis, that almost every new hydroxyl formed subsequently on crosslinker or alkylating agent reacted further, when the molar ratio of CMC/H_2O/NaOH/epichlorohydrin/ GTMAC = 1:500:20:10:5 is used. This is known from our previous derivation studies on different polysaccharides and lignocellulose materials (Simkovic et al. 2011, 2014, 2015, 2017).

NMR analysis

There is a previous report on the NMR data of CMC Na with DS ∼ 0.7 (Kono 2013). Their spectra were run at 343 K using sodium trimethylsilylpropanesul-fonate (DSS) as internal standard. According to our heteronuclear single quantum correlation (HSQC) experiment (Fig. 1; DS ∼0.7), run at 313 K with 3-(trimethylsilyl)-2, 2, 3, 3-tetradeutero-propionic acid (TSP) as internal standard, we observed three anomeric signals at 4.57/104.98, 4.63/104.83 and 4.80/103.22 ppm [see supporting information (SI), Table S1 and Fig. S1 on top]. We assigned the highest signal at 4.57/104.98 ppm to unsubstituted cellulose. We assigned the second peak, with slightly lower intensity at 4.63/104.83 ppm to 1 2-O-CMC, and the peak at 4.80/103.22 ppm to 1 6-O-CMC unit (Fig. 1). According to previous studies, the exact shifts of ano-meric signals depend on the type of cycle, i.e. Na^+ cycle (Kono 2013; 2016 a, b), or Li^+ cycle (Qiu et al. 2014). In our case, there was a Na+ form at DS ∼ 0.7 confirmed by the results of correlation spectroscopy (COSY) showed in Fig. S2 (SI), HSQC shown in Fig. 1, HSQC-TOCSY showed in Fig. S3 in SI, and heteronuclear multiple bond correlation (HMBC) showed in Fig. S4 (SI). Based on the HSQC spectrum, the chemical shifts at 3.87/71.60 ppm were assigned to -CH_2-COO- substituent. Differently substituted carboxymethyl groups have a peak at 4.00/73.21 ppm, whereas the third type of CM-groups were observed at 4.11-4.34/73.94 ppm (Kono, at al. 2016 a; b). HSQC-TOCSY spectrum (Fig. S2, SI) is identical with analogous spectrum published by Kono (2013). Also, signals indicating the presence of 3, 6-Di-O-CMC and 2, 3, 6-trisubstituted-O-CMC units were observed in the spectrum of DS∼0.7 sample. The same results were confirmed also by Kono (2013) on their CMC Na sample with the same DS ∼0.7. Further, HMBC spectrum (Fig. S3, SI) presents carboxyl groups signal at 4.10/180.89

due to -CH_2-COONa interaction of 6-O-CM. The other assigned interaction at 3.99/180.50 ppm is analogous, but related to 2-O-CM substitution.

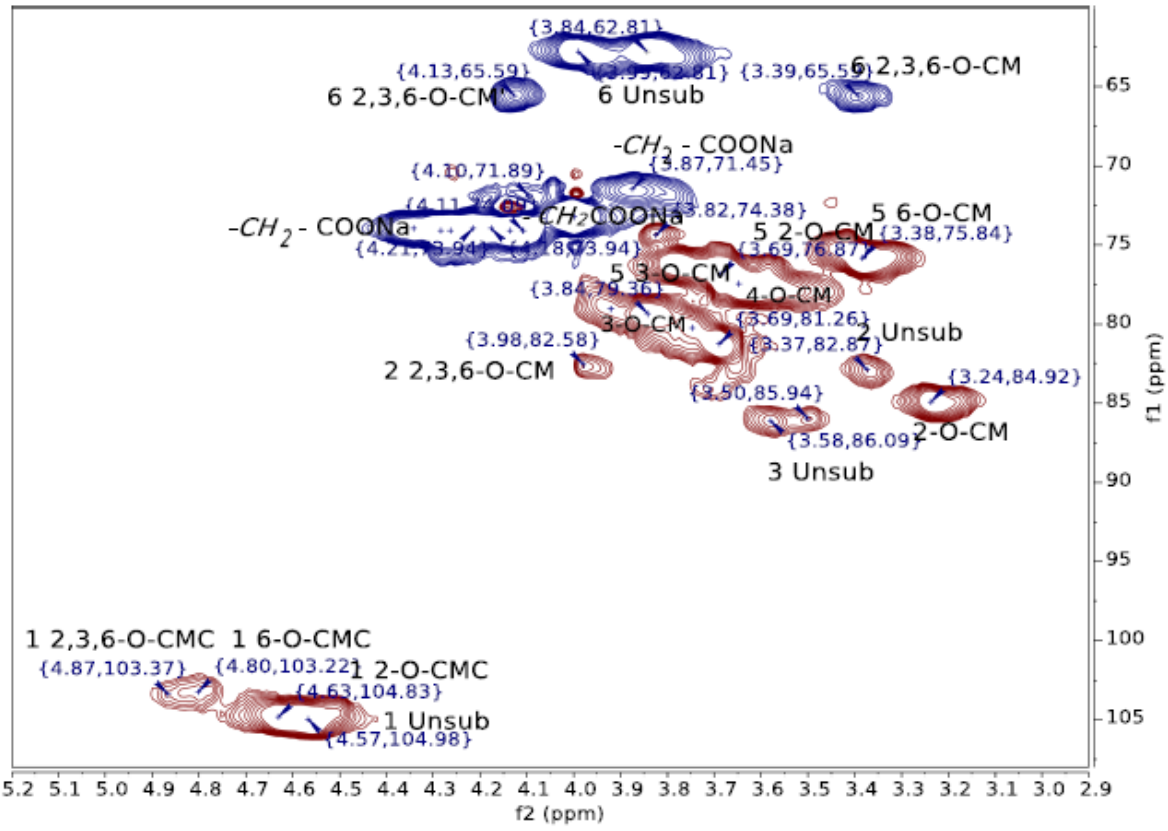

Fig. 1 HSQC spectrum of CMC Na

The QCMC derivative (Fig. S1, the second drawing from top) was obtained at 116% yield. HSQC spectrum (Fig. 2, Table S1) contains the most intense signal at 3.24/56.95 ppm, which belongs to the $(CH_3)_3$ group linked to quaternary nitrogen. The other signals of the spacer are at 3.60/66.47 [-CH_2-$N^+(CH_3)_3$], 3.61/75.99 (-CH_2-O-R) and 4.43/67.79 or 4.29/69.25 (-CH-OH) ppm. The data indicate that the COSY (Fig. S5) anomeric signal of quat-ernized substituent at 4.76 ppm is overlapped with the peak which has spin-spin interaction with a peak at 3.61 ppm (assigned to H_2 of the quaternized ring with C_2 at 77.60 ppm according to HSQC). The signal at 4.76 ppm is not present in CMC Na COSY spectrum (Fig. S2). The anomeric signal related to quaternized/carboxymethylated anomeric signal is at 4.76/103.08 ppm. The other anomeric signals were found at 4.56/104.98 ppm (H1/C1 2-O-CM), and 4.59/104.83 ppm (H_1/C_1 unsubstituted QCMC unit). HSQC-TOCSY spectrum (Fig. S6) showed the signal at 4.91/64.71 ppm proving the linkage of the quaternary group to C_6 (Table S1). The substitution of the quaternary group is also at the C_2-position, which was confirmed by HMBC experiment (Fig. S7), in particular by the signal at 3.60/76.02 ppm (-CH_2-O-C_2). The pattern of the signals at 4.33/181.67, 4.27/180.69, 4.20/181.28, 4.15/180.69, 4.10/180.89, and 3.99/180.50 ppm was identical with the CMC Na sample.

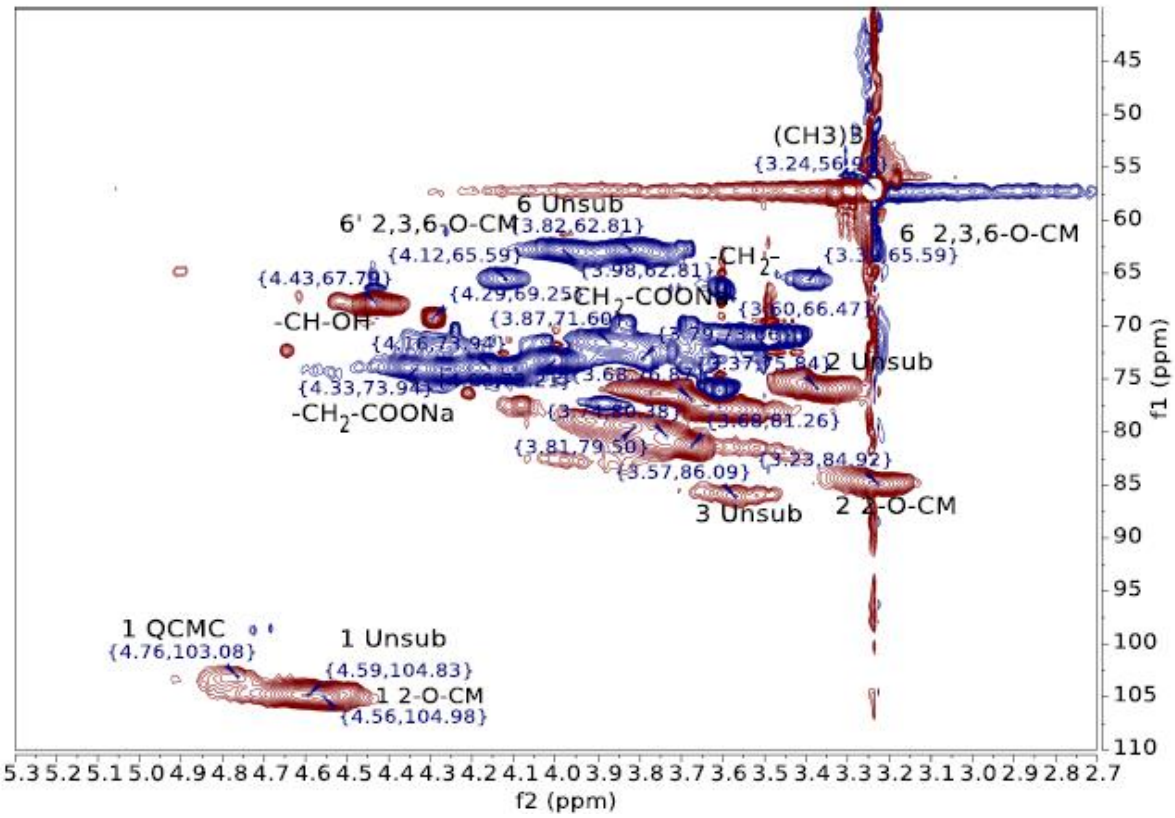

Fig. 2 HSQC spectrum of QCMC

The crosslinked CMC Na (CCMC; structural drawing shown in Figure S1, second from the bottom; 121% yield) was assigned analogously as described earlier using the combination of COSY (Fig. S8), HSQC (Fig. 3), HSQC-TOCSY (Fig. S9), and HMBC (Fig. S10). The anomeric region consisted of four signals at 4.57/104.83 (unsubstituted CMC Na), 4.60/104.83 (2-mono-O-CM unit), 4.77/103.08 (crosslinked-O-CMC Na unit), and 4.79/103.08 ppm (6-mono-O-CMC unit). The chemical shifts of 2-hydroxypropyl linker are at 3.42, 3.84/69.58 or 4.24, 4.28/74.09 ppm [CMC-O-CH_2-CH(OH)-CH_2-O-CMC] with the -CH(OH) group at 3.92/73.35 or 4.04/71.74 ppm. The -CH_2-COO- of mono-, di- and tri-substituted signals are at 3.84/71.74 and 3.66/73.2 ppm similarly as described for CMC Na case.

According to the HSQC spectrum (Fig. 4), the crosslinked and quaternized CMC Na (QCCMC; 122% yield) sample (hypothetical structure shown in the Figure S1, bottom), showed four anomeric signals at 4.60/104.83 (unsubstituted QCCMC), 4.73/102.64 (CMC-O-crosslinked-O-CMC), 4.82/103.22 (6-mono-O-Q), and 4.85/103.47 (6-mono-O-CM). The mixed di-substituted and tri-substituted rings have similar DS. All signals were assigned by comparing with anomeric signals of CMC Na, CCMC, and QCMC samples. COSY (Fig. S11) and HSQC spectra enabled assignment of four types of C_6 types of CH_2 signals, (Table S1). In a similar way also H_3/C_3 and H4/C4 could be assigned. The signals of H_5/C_5 and H_6/C_6 could be assigned from the HSQC, HSQC-TOCSY, and HMBC results. The signals of the quaternary spacer are at 3.23/56.95 ppm [$N^+(CH_3)_3$], 3.60/66.47 [-CH_2-$N^+(CH_3)_3$], 3.61/75.84 [-CH_2-O-R] and 4.90/64.86 [-CH-OH] ppm. The 2-hydroxypropyl crosslinker is at 3.60, 3.67/75.84 ppm [R_1-CH_2-CH(OH)-CH_2-R_2] with -CH(OH) at 3.90/73.35 ppm. In the HSQC-TOCSY (Fig. S12) spectrum, the peak at 3.91/65.34 ppm is in correlation with peaks at 3.60/66.47 and 3.66/65.34 ppm, confirming the linkage of the -CH_2-CH(OH)-CH_2-crosslinker. In the HMBC (Fig. S13) spectrum of QCCMC, there are several carboxyl-related signals at 4.35/181.47, 4.09/180.69, and 3.99/180.30 ppm resulting from the -CH_2-

COO- interaction. In addition, the peaks at 4.43/70.95 and 4.43/76.02 ppm confirmed the presence of the -CH(OH)-CH_2- group in quaternized spacer.

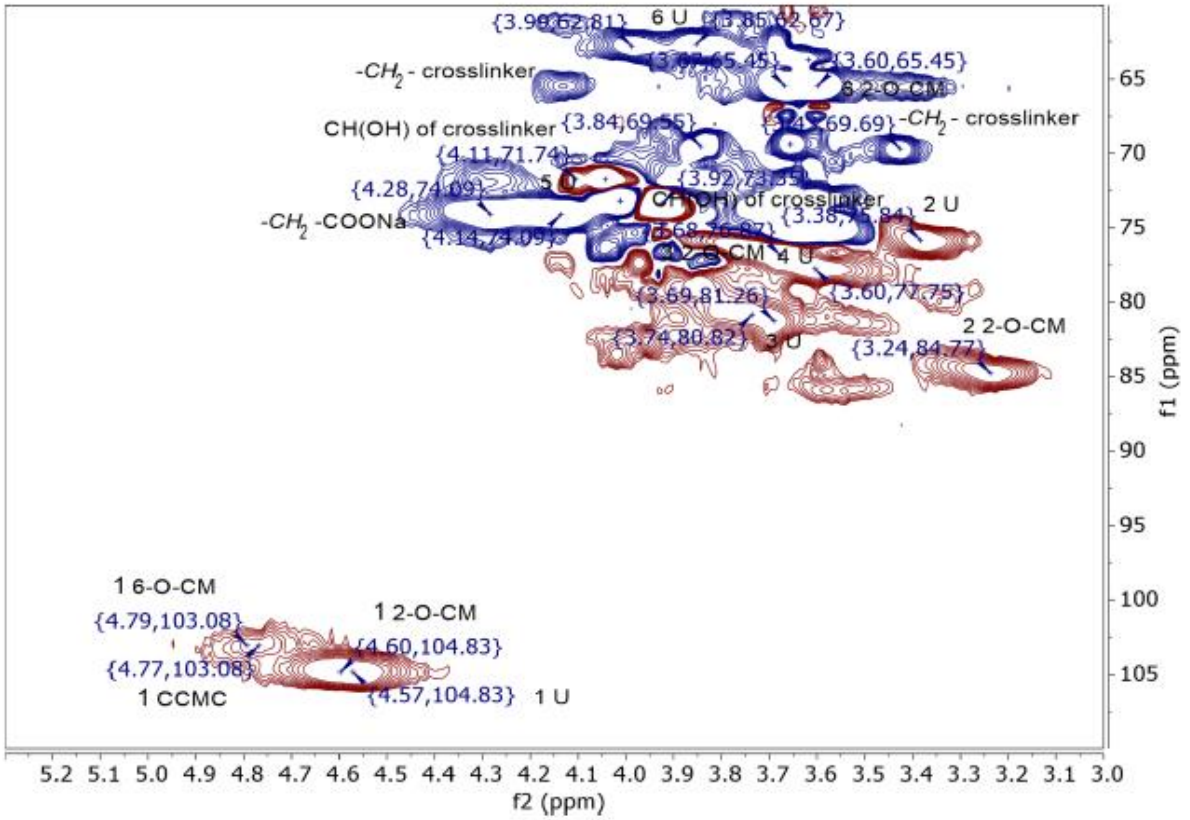

Fig. 3 HSQC spectrum of CCMC

SEC-MALS analysis

SEC-MALS characterization was performed in both carbonate (0.1 M Na_2CO_3 pH 10.0) and in an acetate buffer (0.1 M CH_3COONa buffer pH 4.5). Due to the better results of recovered mass for CMC Na (98.2%) > CCMC (81.2%) > QCMC (78.2%) > QCCMC (77.4%), we used the data obtained at pH 10 (Fig. 5). The molecular weights at the peak were similar for all four derivatives: CCMC (31.2 kg/mol) > CMC Na (30.5 kg/mol) > QCMC (30.4 kg/mol) > QCCMC (28.7 kg/mol). The size of all four polysaccharides macromolecules (i.e. radius of gyration, R_g) were in the nano-scale (< 100 nm). It is apparent that the R_g values of the QCMC, CCMC, and QCCMC were smaller than that of CMC Na. The average molecular weight (M_w) at the point where all four curves are crossing each other was at 80 kg/mol. The M_w of the four studied samples were decreasing in the following order: QCCMC > QCMC > CMC Na > CCMC. The water solubility of studied derivatives were found to be decreasing in the following order: CMC Na (98.0%) > CCMC (81.2%) > QCMC (78.2%) > QCCMC (77.4%). The fact that CCMC sample was more soluble than QCMC and QCCMC samples indicates ionic interactions between carboxyls and quaternary ammonium groups.

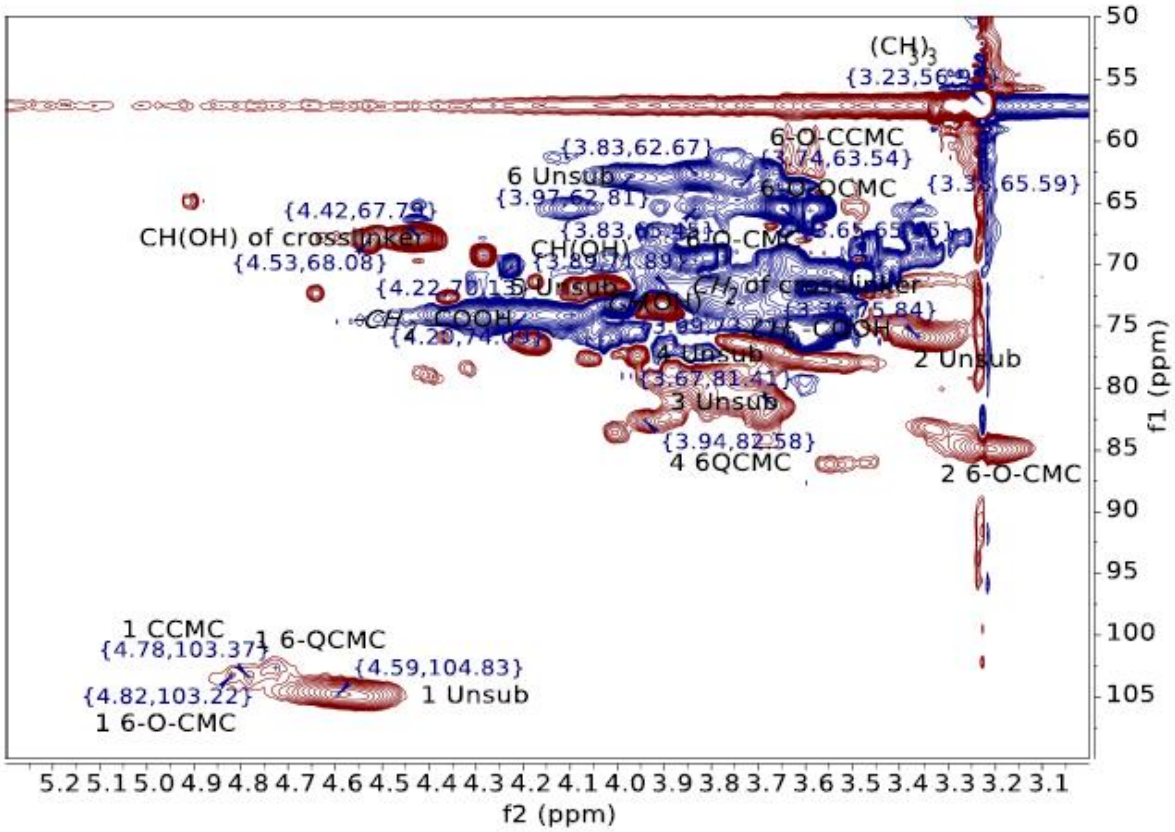

Fig. 4 HSQC spectrum of QCCMC

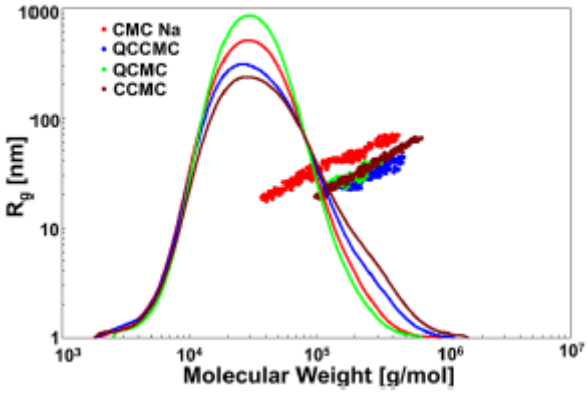

Fig. 5 Conformation plot $R_g = f(M)$ comparison of CMC Na and QCMC, CCMC, QCCMC

Figure 5 shows comparison of conformation plot -$R_g = f(M)$: R_g=size, M = molecular weight - of CMC Na and of QCMC, CCMC and QCCMC derivatives. MALS is an elastic or total intensity light scattering detector and macromolecules size R_g is obtained from the angular variation of scattered light. By MALS the minimum measurable R_g is approximately 15 nm. Analyzing Fig. 5, it is evident that size R_g of derivatives (QCMC, CCMC, QCCMC) with respect to the CMC Na sample at constant molecular weight

is meaningful lower; in other words the derivatives conformation is more compact respect to CMC Na. Furthermore, the QCCMC sample has little more compact conformation.

We expect the R_g values play a crucial role in film formation; by decreasing the radius of polysaccharides coils, their interaction potential increases. During the process of film formation, the water gradually evaporates, bringing the coils closer to each other and allowing them to interact. Ionic and hydrogen bond interactions are expected to represent the most prevalent kind. Besides hydroxyl groups, CMC Na and CCMC contain only carboxyl groups, while QCMC and QCCMC also contain quaternary ammonium group. According to this we expect that the interactions between carboxyls and quaternary ammonium groups results in smaller R_g values and shorter distances and stronger interactions between individual coils in the prepared films.

Electrochemical measurements

Cyclic voltammograms acquired with electrodes coated by the modified CMCs are in the Fig. 6. Since a negatively charged probe (ferricyanide) was employed, presumably any electrode coating with negatively charged moieties will cause decrease in CV peak height as well as larger separation between the anodic and the cathodic peak (ΔE). This expectation was confirmed, considering the unmodified SPE exhibited ΔE of 252 mV while CCMC coating increased AE to 302 mV. CMC Na sample exhibited a similar value of ΔE=292 mV. It can be ascribed to the presence of dissociated carboxyls in CMC Na, which hinder negatively charged ferricyanide, displaying as a larger potential needed for its electrochemical oxidation and reduction. On the other side QCMC where positively charged groups were introduced, facilitated diffusion of ferricyanide ions to the electrode surface, which displayed as the ΔE = 161 mV. Accordingly, both anodic (I_a) and cathodic (I_c) peak heights were significantly lower at CMC Na and CCMC compared to unmodified SPE or SPE modified with QCMC or QCCMC (see Table 1).

Table 1 Parameters E, Ia and Ic acquired from third scans of cyclic voltammograms measured with individual electrodes denoted in the first column

Electrode	ΔE (mV)	I_a (μA)	I_c (μA)
SPE	252	83.90	−88.95
SPE-CMC Na	292	63.84	−66.65
SPE-CCMC	302	64.78	−69.26
SPE-QCMC	161	98.31	−104.65
SPE-QCCMC	201	91.20	−95.01

The results are in good agreement with previously observed modulation of ferricyanide redox transformation rate by the coating of a carbon electrode with quaternized chitosan mixed with various amounts of negatively charged xylan (Simkovic at al., 2018). It should be noted that the voltammograms and respective parameters acquired with modified SPEs may suffer bias caused by very good solubility of all CMC derivatives in aqueous solutions, which is the reason why even with CMC-coated SPE relatively high Ia and Ic were observed, compared to electrodes modified with xylan.

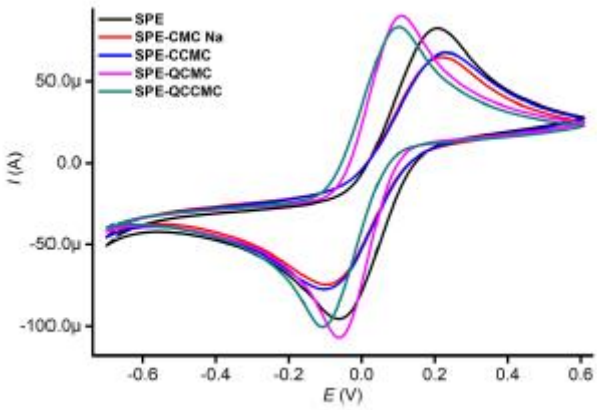

Fig. 6 Cyclic voltammograms of unmodified SPE (black) and SPEs modified with CMC Na (red), CCMC (blue), QCMC (magenta) and QCCMC (green). Voltammograms were acquired in 150 µL of PB + 10 mM ferricyanide at a scan rate of 100 mV s^{-1}. Third scans are shown

XRD analysis

Figure 7 shows the symmetric XRD scans of CMC Na, CCMC, QCMC, and QCCMC; the amorphous state of all four films can be concluded.

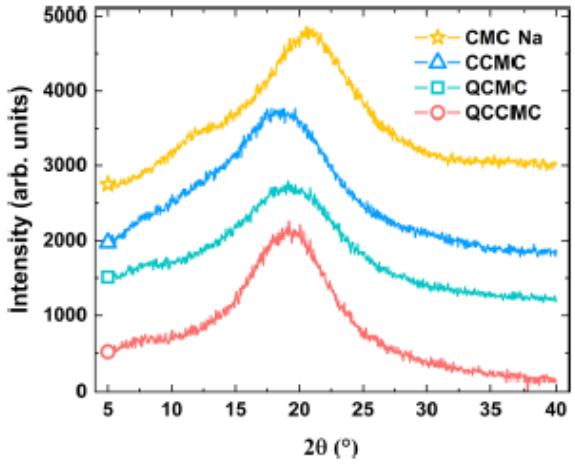

Fig. 7 Symmetric XRD scans of CMC Na, CCMC, QCMC, and QCCMC films (from top to bottom)

A dominant broad band at ~20.5° and a weak band ~12° observed in the CMC Na film indicate there was no crystalline cellulose in pure form (Kumar et al. 2020). Traces of CII cannot be completely ruled out however, since the three most intense CII reflections with Miller indices of (1-10), (110), and (020) are expected to be located at respective 20 angles of 12.0°, 20.0°, and 22.0° (Kuang et al. 2020; French 2014), and may be completely screened by the observed broad band. Interestingly, the main broad band slightly shifted to smaller 20 angles, i.e. ~18.4° for CCMC and ~19.1° for both QCMC and QCCMC. A weak band observed in CMC Na film at ~12° was not observed in any other film. However, weak signs of the band located at ~8° were observed in QCMC and QCCMC films.

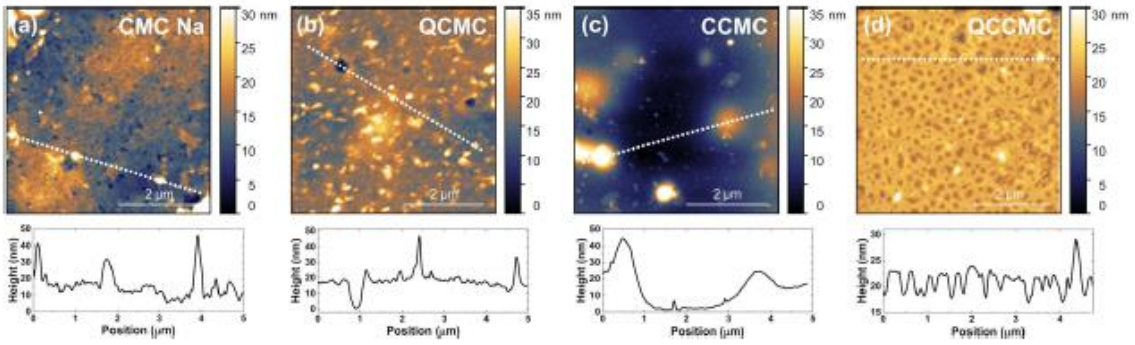

Fig. 8 Representative 5 µm X 5 µm AFM topography scans with corresponding line profiles extracted along the designated white dotted lines of a CMC Na, b QCMC, c CCMC, and d QCCMC films

PF-QNM analysis

Surface morphology and mechanical properties of CMC Na, QCMC, CCMC, and QCCMC films are discussed in this section. Using PF-QNM technique, spatially resolved reduced elastic modulus, stiffness, and adhesion were determined. Histograms for all of these quantities were calculated to obtain the distributions of measured values. Gaussian peak fitting was used to determine the mean values. We note that determining mechanical properties are limited to the surface of the prepared films (indentation depth $\leq$ 10 nm) and their bulk values may be significantly different.

Surface morphology

Representative topography scans of all prepared films are shown in Fig. 8 (a-d). Also shown are corresponding line profiles taken along the white dotted lines shown in the topography maps. All films were found relatively smooth; following RMS surface roughness values were found: CMC Na (6.4 nm) > CCMC (6.5 nm) > QCMC (4.1 nm) > QCCMC (2.0 nm). Particles several tens of nm tall and several hundreds of nm wide were found scattered across the surfaces of all measured samples with various densities, which was highest in the QCMC film. The surface of the CCMC film showed a wavy-like surface with valleys several qm wide and several tens of nm deep. It seems that CCMC particles have the biggest dimension in comparison to the other three samples. The particle dimensions were the lowest for QCCMC (but similar to CMC Na and QCMC) film and the surface was porous with homogeneously distributed pores about 2-5 nm deep and approximately 100-300 nm wide.

Reduced modulus

Reduced modulus maps of all four studied films along with the corresponding statistical distributions of obtained values are shown in the Fig. 9 (a-d); the mean values were determined from Gaussian fitting. Following decreasing order was found: CCMC (9.3 GPa) > QCCMC (8.0 GPa) > CMC Na (7.0 GPa) > QCMC (2.1 GPa). Patches of lower values of reduced modulus were observed in all four films and these roughly correlated with the locations, where the particles discussed in the previous section were observed (Fig. 8). These particles may be dependent on the density of crosslinking of individual samples. CMC Na and QCMC were not crosslinked and showed lower modulus values than QCCMC and CCMC; CCMC had the highest crosslinking density.

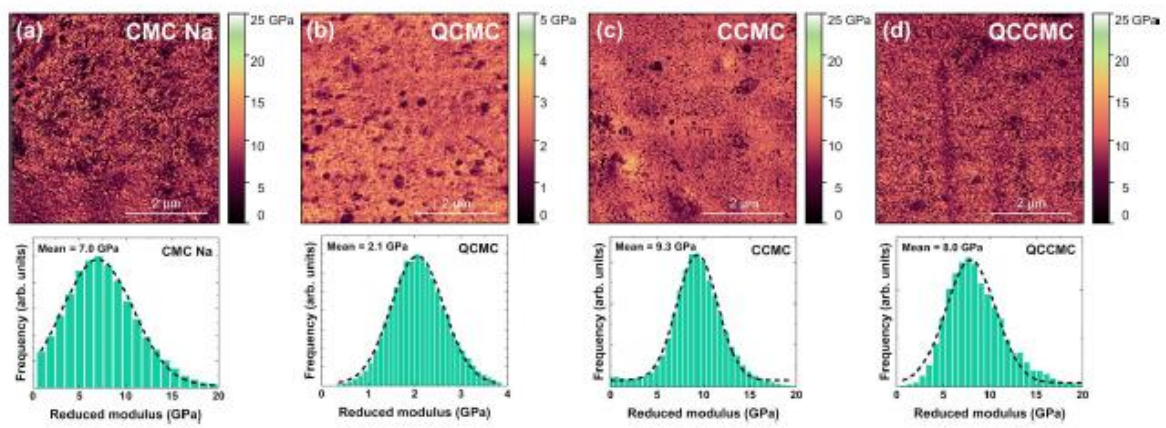

Fig. 9 PF-QNM reduced elastic modulus maps of a CMC Na, b QCMC, c CCMC, and d QCCMC films

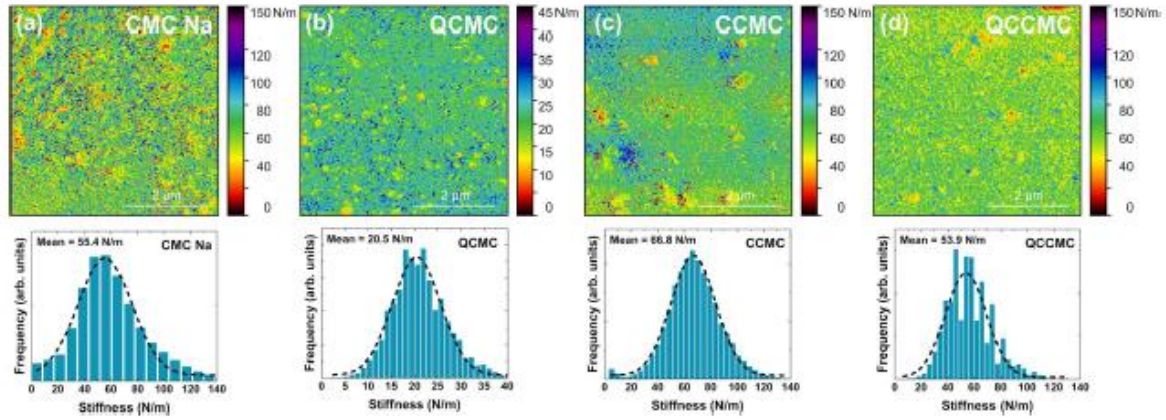

Fig. 10 PF-QNM stiffness maps of a CMC Na, b QCMC, c CCMC, and d QCCMC films

Stiffness

Figure 10 (a-d) show PF-QNM-determined stiffness maps of all four studied films and their corresponding statistical distributions; the mean values were determined from Gaussian fitting. Following decreasing order of stiffness was found: CCMC (66.8 N/m) > CMC Na (55.4 N/m) > QCCMC (53.9 N/m) > QCMC (20.5 N/m), which almost matches that of the reduced modulus. Here, the order of CMC Na and QCCMC films are exchanged, however their corresponding respective stiffness values of 55.4 N/m and 53.9 N/m were similar and the difference is within the uncertainty of the measurement. Again, patches of lower stiffness values coinciding with the patches of lower values of reduced modulus (Fig. 9) and the location of particles (Fig. 8) were observed. We consider the determined stiffness values also the result of the crosslinked density of individual samples. The stiffness might reflect more the repulsion of identical ions of CMC Na and CCMC samples, than opposite ions interaction present in QCCMC and QCMC samples.

Adhesion

Spatially resolved PF-QNM-determined adhesion maps of CMC Na, QCMC, CCMC, and QCCMC films are presented in Fig. 11 (a-d). These represent the work of adhesion required for the probe to detach from the surface at a particular measured pixel and at the nanoscale is typically caused by van der Waals, capillary, and electrostatic forces. Also shown in Fig. 11 are corresponding statistical distributions; the mean values of adhesion were determined from Gaussian fitting. Following decreasing order of mean adhesion was found: CCMC (25.7 nN) > CMC Na (21.4 nN) > QCMC (17.1 nN) > QCCMC (11.5 nN).

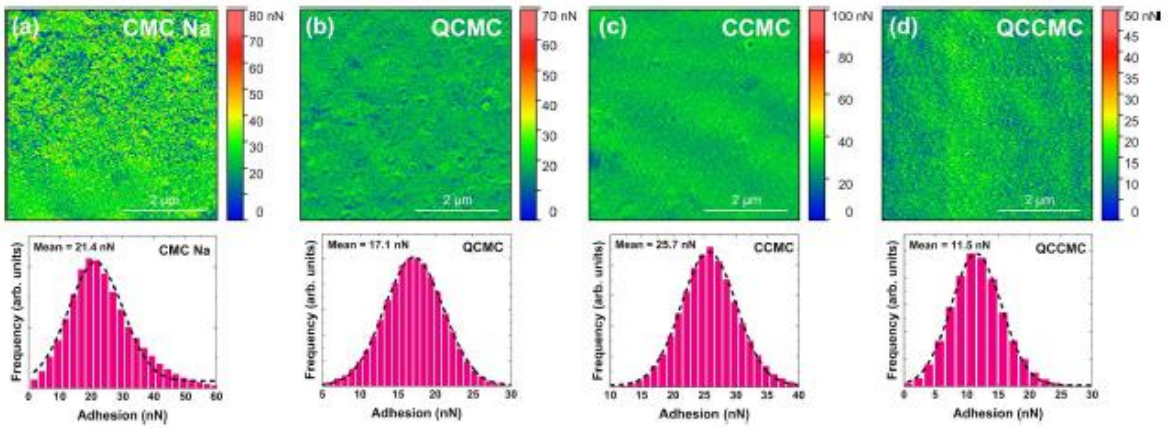

Fig. 11 PF-QNM adhesion maps of a CMC Na, b QCMC, c CCMC, and d QCCMC

CMC Na and CCMC, and QCMC and QCCMC films showed comparable mean adhesion values suggesting some extent of surface similarities between the two groups of films. While CCMC and CMC Na samples contain only one type of charge ($COO^{-}Na^{+}$), there are two types of charges in QCMC and QCCMC samples, as could be seen in the chemical structures presented in SI part of the manuscript. The mean adhesion difference between the two groups was ~50-100%. Similar to reduced modulus and stiffness, patches of lower adhesion values roughly matched some of the locations of patches of lower values of stiffness (Fig. 10), reduced modulus (Fig. 9), and location of particles (Fig. 8) were observed.

In comparison to results observed on seaweed films (Simkovic et al. 2021), the roughness values were distributed on broader scale, from 18.6 nm (Fur-cellaran) > 14.0 nm (Gigartina Skottsbergi ultrasound water extract (GSUW) > 8.0 nm (GSW) > 5.5 nm (i-carrageenan) > 5.2 nm (GS ultrasound carbonate peroxide extract (GSUCP) > 2.4 nm [(Furcel-laria lumbricalis water extract (FLW)]. The reduced modulus values were significantly smaller for seaweeds [FLW (1685 MPa) > GSUW (822 MPa) > Fur-cellaran (817 MPa) > GSUCP (807 MPa) > K-carrageenan (433 MPa) > GSW (378 MPa) > i-carrageenan (24 MPa)] than observed for cellulose derivatives [CCMC (9.3 GPa) > QCCMC (8.0 GPa)> CMC Na (7.0 GPa) > QCMC (2.1 GPa)]. The stiffness values of CCMC (66.8 N/m) > CMC Na (55.4 N/m) > QCCMC (53.9 N/m) were of the same order (except for the i-carrageenan), but mostly higher (~2-5 times) [FLW (23.1 N/m) > GSUW (14.4 N/m) > GSUCP (13.5 N/m) > Furcellaran (13.2 N/m) > GSW (11.5 N/m) > K-carrageenan (10.7 N/m) > i-carrageenan (0.8 N/m)] than determined on seaweeds. The adhesion values of CCMC (25.7 nN) > CMC Na (21.4 nN) > QCMC (17.1 nN) > QCCMC (11.5 nN), were also similar compared to seaweeds [GSW (22.1 nN) > FLW (15.0 nN) > GSUUCP (14.5 nN) > GSUW (9.4 nN) > Furcellaran (7.3 nN) > i-carrageenan 4.7 nN) > K-carrageenan (4.5 nN)]. Clearly, there are several factors affecting the

differences, with a much higher charge of seaweed polysaccharides, which allows the macromolecules with higher M_w to be solubilized in water than for CMC derivatives. The differences in conformations of the two groups indicate that the seaweeds are more regularly ordered in water, while the QCMC and QCCMC derivatives behave differently due to the presence of both carboxyls and quaternary ammonium groups acting with repulsion and ionic crosslinking forces against each other. This was indicated on the basis of cyclic voltammograms measurements, which were differently shifted for all four CMC derivatives.

Conclusion

Three new cellulose derivatives were prepared by one-step synthesis from CMC Na by quaterniza-tion, crosslinking, and a combination of quaterniza-tion and crosslinking. The structures of newly prepared compounds were confirmed by high-resolution NMR spectroscopy. The SEC-MALS analysis of CMC derivatives indicated only a slight drop in their water solubility. Macromolecules size R_g values at the constant molecular weight decrease in the following order: CMC Na > CCMC $\geq$ QCMC > QCCMC. Symmetric XRD scans confirmed that films of all four derivatives were in amorphous form. Cyclic voltammograms distinguished all four derivatives with constant ΔE, I_a and I_c parameters. Surface mechanical properties varied significantly. Reference sample CMC Na showed a reduced modulus of 7.0 GPa and stiffness of 55.4 N/m. CCMC film showed the highest reduced modulus of 9.3 GPa and stiffness of 66.8 N/m, while the QCMC film showed much lower values, i.e. 2.1 GPa and 20.5 N/m, even lower than the reference CMC Na film. Similar mean adhesion values of CMC Na and CCMC (21.4 nN vs. 25.7 nN) and QCMC and QCCMC (17.1 nN vs. 11.5 nN) suggest surface similarities between the two groups of films. Particles with different properties were observed across all films. Their positions roughly coincided with patches of lower values of reduced modulus, stiffness and adhesion. The exact origin of these species is not clear, however, based on their observation also on the reference CMC Na film, we believe that they may be related to the CMC Na and not necessarily to the process of quaternization, crosslinking or their combination. Described films may find environmentally-friendly applications e.g. in industrial packaging technology, where some of the dominant plastic materials could be replaced by those made from CMC Na which can be sourced from renewable natural sources.

References

Beghetto V, Gatto V, Conca S, Bardella N, Buranello C, Gasparetto G, Sole R (2020) Development of 4-(4,6-dimethoxy-1,3,5-triayin-2-yl)-4-methyl-morpholin-ium chloride cross-linked carboxymethyl cellulose films. Carbohydr Polym 249:116810. https://doi.org/10.1016/J. CARPOL.2020.116810

Behra JS, Mattson J, Olivier J, Cayre EJ, Robles ESJ, Haiqiu T, Hunter TN (2019) Characterrization of sodium carboxy-methyl cellulose aqueous solutions to support complex product formulation: a rheology and light scattering study. ACS Appl Polym Matter 1:344-358. https://doi.org/10. 1021/acsapm.8b00110

Chang C, He M, Zhou J, Zhang L (2011) Swelling behaviors of pH- and salt-responsive cellulose-based hydrogels. Macromolecules 44:1642-1648. https://doi.org/10.1021/ ma10280f

Choi YJ, Simonsen J (2006) Cellulose nanocrystals-filled carboxymethyl cellulose nanocomposites. J Nanosci Nano-technol 6:633-639. https://doi.org/10.1166/jnn.2006.132

French AD (2014) Idealized powder diffraction patterns for cellulose polymorphs. Cellulose 21:885-896. https://doi. org/10.1007/s 10570-013-0030-4

Gao Y, Li Q, Shi Y, Cha R (2016) Preparation and application of cationic modified cellulose fibrils as a papermaking additive. Int J Polym Sci. https://doi.org/10.1155/2016/ 6978434

Javanbakht S, Shaabani A (2019) Carboxymethyl cellulose-based oral delivery systems. Int J Biol Macromol 133:21-20

Johnson KL, Kendall K, Roberts AD (1971) Surface energy and the contact of elastic solids. Proc R Soc Lond A 324:301-313

Kono H (2013) *H and 13 C chemical shift assignment of the monomers that comprise carboxymethyl cellulose. Carbohydr Polym 97:384-390. https://doi.org/10.1016/). carbpol.2013.05.031

Kono H, Oshima K, Hashimoto H, Shimizu Y, Tajima K (2016) NMR characterization of sodium carboxymethyl cellulose: substituent distribution and mole fractions of monomers in the polymer chains. Carbohydr Polym 146:1-9. https://doi.org/10.1016Zj.carpol.2016.03.021

Kono H, Oshima K, Hashimoto H, Shimizu Y, Tajima K (2016) NMR characterization of sodium carboxymethyl cellulose 2: chemical shifts assignment and conformation analysis of substituent groups. Carbohydr Polym 150:241-249. https://doi.org/10.1016/j.car pol.2016.05.003

Kuang Y, Li X, Luan P, Zhang X, Xu J (2020) Cellulose II nanocrystal: a promising bio-template for porous or hollow nano SiO2 fabrication. Cellulose 27:3167-3179

Kumar B, Deeba F, Priyadarshi R, Sauraj Bano S, Kumar A, Negi YS (2020) Development of novel cross-linked carboxymethyl cellulose/poly (potassium 1-hydroxy acrylate): synthesis, characterization and properties. Polym Bull 77:4555-4570. https://doi.org/10.1007/s00289-019-02985-8

Qiu L, Shao Z, Yang M, Wang W, Wang F, Wan J, Wang J, Bi Y, Duan H (2014) Study on effects of carboxymethyl cellulose lithium (CMC-Li) synthesis and electrospinning on high-rate lithium ion batteries. Cellulose 21:615-626. https://doi.org/10.1007/s10570-013-0108-z Šimkovic I, Gedeon O, Uhliariková I, Mendichi R, Kirsch-nerová S (2011) Positively and negatively charged xylan films. Carbohydr Polym 83:769-775. https://doi.org/10. 1016/j.carbpol.2010.08.047

Šimkovic I, Tracz A, Kelnar I, Uhliariková I, Mendichi R (2014) Quaternized and sulfated xylan derivative films. Carbohydr Polym 99:356-364. https://doi.org/10.1016/j. carpol.2013.08.075

Šimkovic I, Mendichi R, Kelnar I, Filip J, Hricovíni M (2015) Cationization of heparin for film applications. Carbohydr Polym 115:551-558. https://doi.org/10.1016/j.carpol. 2014.09.021

Šimkovic I, Kelnar I, Mendichi R, Bertok T, Filip J (2017) Composite films prepared from agricultural by-products. Carbohydr Polym 156:77-85. https://doi.org/10.1016/j. carbpol.2016.09.014

Šimkovic I, Kelnar I, Mendichi R, Tracz A, Filip J, Bertók T, Kasak P (2018) Interface study of all-polysaccharide interface films. Chem Pap 72:711-718

Šimkovic I, Gucmann F, Mendichi R, Schieroni AG, Pio-vani D, Dobročka E, Hricovíni M (2021) Extraction and characterization of polysaccharide films prepared from Furcellaria lumbricalis and Gigartina skottsbergii seaweeds. Cellulose 28:9567-9588. https://doi.org/10.1007/ s 10570-021-04138-5

Ünlü CH (2013) Carboxymethylcellulose from recycled newspaper in aqueous medium. Carbohydr Polym 97:159-164. https://doi.org/10.1016/j.car pol.2013.04.039 Wang M, Jia X, Liu W, Lin X (2021) Water insoluble and flexible transparent film based on carboxymethyl cellulose. Carbohydr Polym 255:117353. https://doi.org/10.1016/j. carbpol.2020.117353

Wei P, Chen W, Song Q, Wu Y, Xu Y (2021) Superabsorbent hydrogels enhanced by quaternized tunicate cellulose nanocrystals with adjustable strength and swelling ratio. Cellulose 28:3723-3732. https://doi.org/10.1007/ s10570-021-03776-z

Zennifer A, Senthilvelan P, Sethuraman S, Sundaramurthi S (2021) Key advances of carboxymethyl cellulose in tissues engineering & 3D bioprinting applications. Carbohydr Polym 256:117561. https://doi.org/10.1016/j.carpol. 2020.117561 https://www.brukerafmprobes.com/p-3365-nchv.aspx